Cement and Concrete Research 42 (2012) 252–264

Contents lists available at SciVerse ScienceDirect

Cement and Concrete Research

journal homepage: http://ees.elsevier.com/CEMCON/default.asp

The effect of segregation on transport and durability properties of self consolidating concrete

D.K. Panesar *, B. Shindman

Department of Civil Engineering, University of Toronto, 35 St. George St., Toronto, Ont., Canada M5S 1A4

ARTICLE INFO

Article history:
Received 11 June 2011
Accepted 23 September 2011

Keywords:
Durability (C)
Dynamic and static segregation (C)
Stability (C)
Transport properties (C)
Mechanical properties (C)

ABSTRACT

Considerable effort has been placed on the development of reliable and practical tests to reflect segregation behavior because it is a critical property for successful application of self-consolidating concrete (SCC). This investigation examines segregation performance measured based on the column method, visual stability index and V-funnel (t_5–t_0) tests and assesses their correlation to mortar band thickness, compressive strength, rapid chloride permeability, initial sorptivity coefficient, freeze–thaw and salt scaling performance. The primary outcomes from this study reveal that: (i) freeze–thaw resistance of the studied SCC mixtures is controlled by air entrainment irrespective of the extent of segregation; (ii) a wide range of mortar band thicknesses occurs at the specified acceptable segregation limit; (iii) accurate mortar band analysis using digital images requires strong contrast and brightness at the aggregate–paste boundary, and an experimental approach for sample preparation and analysis is proposed; and (iv) the correlation between mortar band thickness, sorptivity and salt scaling mass loss is directly proportional.

1. Introduction

Stability is the most important plastic property for successful application of self consolidating concrete (SCC) technology. Due to the high flowability of SCC, it is much more susceptible to stability problems than conventionally consolidated concrete, particularly if it is not proportioned to be cohesive [1]. Stability, also referred to as segregation resistance, is the ability of a SCC mixture to retain a uniform distribution of all constituent materials during the casting process and once all placement and casting operations have been completed. The former is referred to as dynamic stability and the latter as static stability [2]. Dynamic instability can be caused by the input of any form of vibration energy into the system during material transport or placement [3]. Static stability is the ability of concrete to resist bleeding, segregation and settlement, which are influenced by gravity and time. Instability can result in differential accumulation of light components and settling of aggregate, leaving a mortar layer on top of the concrete [4]. Although static segregation can easily be detected by visual inspection if there is excessive bleeding, it becomes more difficult to detect if the bleed water is not visually apparent due to the difficulty of water to travel along bleeding channels in viscous SCC systems [3,5,6]. Visually apparent bleed water or not, the extent of movement and distribution of coarse aggregate, air and water that occurs during concrete mixing and placing or after placement has implications on the laboratory measured mechanical, transport and durability properties of SCC and also the in situ properties, which can result in dramatic effects on reinforced concrete structures [3,6–8]. Beyond the inhomogeneity of the aggregate distribution, instability can also weaken the interface between the aggregate and the cement paste, and can adversely affect the bond behavior between steel and concrete [9,10]. SCC mixtures are designed with a higher volume of paste which is more susceptible to shrinkage cracking in comparison to conventional concrete [11]. Segregated SCC has a higher cracking risk due to aggregate settlement which leaves a top layer richer in paste, which may experience more shrinkage in comparison with unsegregated concrete. Unstable SCC can experience weak cement–aggregate interface, poor bond behavior and shrinkage effects acting alone or simultaneously. This can increase the vulnerability of reinforced concrete structures to microcracking, which is of particular concern related to the long term durability performance. Cracking due to segregation can reduce the resistance of concrete to the ingress of moisture and ions and, if exposed to freeze–thaw temperatures, can further promote increased permeation and reduced mechanical properties impairing the structures' integrity.

Although in general, the hardened properties of SCC are at least as good as, if not superior to those of conventionally vibrated concrete [12–19], few studies have identified which qualitative or quantitative measures of segregation correlate with the concrete's transport and durability properties. Currently, several test methods can be used to directly or indirectly measure segregation. Static and dynamic segregation can be evaluated by the screen stability test, column segregation test,

* Corresponding author. Tel.: +1 416 946 5712; fax: +1 416 978 6813.
E-mail addresses: d.panesar@utoronto.ca (D.K. Panesar), benjamin.shindman@utoronto.ca (B. Shindman).

0008-8846/$ – see front matter © 2011 Elsevier Ltd. All rights reserved.
doi:10.1016/j.cemconres.2011.09.011

V-funnel (t_5–t_0) and visual stability index (VSI) [20–22]. The latter three measures of segregation are specified by the Ministry of Transportation of Ontario (MTO) and are considered in this study. In addition, direct determination of segregation stability of SCC can be assessed by measuring the depth of sedimentation of the upper layer of coarse aggregate particles, or by the fraction of coarse aggregate with specimen height. This paper details the development of an experimental procedure using digital image analysis to analyze the mortar band thickness, which is compared with the column segregation, VSI and V-funnel (t_5–t_0) measurements.

The objective of this study is to evaluate the implications of segregation on the concrete's compressive strength, rapid chloride permeability, initial sorptivity, freeze–thaw resistance and de-icer salt scaling resistance. The significance of identifying the correlations between plastic, hardened, and durability properties forms the basis for identifying indicators of durability performance that can provide early detection of substandard quality SCC, which can shorten a structure's life. These outcomes complement current advances in SCC research and parallels research initiatives currently underway related to identifying durability indicators [23].

2. Experimental program

2.1. Materials and mix design

2.1.1. Materials

The cementing materials used were general use (GU) cement and ground granulated blast furnace slag (GGBFS), which was used as a supplementary cementing material. The chemical composition and physical properties of the cementing materials are presented in Tables 1 and 2, respectively.

The specific gravity, fineness modulus and absorption of the fine aggregate, which is a natural sand, were experimentally determined to be 2.7, 2.8 and 1.5%, respectively. The coarse aggregate is a crushed limestone with a nominal maximum size of 13 mm. Two coarse aggregate gradations were used. Gradation A falls in the middle of the upper and lower gradation limits of Ontario Provincial Standard Specification (OPSS) 1002/ASTM C33-07 [24,25] and Gradation B is equal to the lower limit of OPSS 1002/ASTM C33-07 [24,25]. The specific gravity and absorption of the coarse aggregate are 2.7 and 1.3%, respectively.

The superplasticizer is a polycarboxylate based high range water reducing admixture with a specific gravity of 1.064. The air entraining admixture used is MicroAir, and it has a specific gravity of 1.010. The liquid viscosity modifying admixture used is Rheomac 362, which has a specific gravity of 1.002.

Table 1
Chemical composition of cementing materials.

Constituent	GU (% by mass)	GGBFS (% by mass)
SiO_2	19.24	37.24
Al_2O_3	5.43	8.70
Fe_2O_3	2.36	0.35
CaO	60.94	37.94
MgO	2.34	11.36
SO_3	4.11	2.68
K_2O	1.11	0.43
Na_2O	0.22	0.43
TiO_2	0.26	0.48
SrO	0.08	–
P_2O_5	0.1	0.02
Cl	0.03	0.01
ZnO	0.02	–
Cr_2O_3	0.01	0.11
Mn_2O_3	0.06	0.46
Leco CO_2	2.22	0.38
Leco SO_3	3.95	2.16
Free lime	1.10	2.16

Table 2
Physical properties of cementing materials.

Property	GU	GGBFS
Density (kg/m^3)	3120	2870
LOI 1000 °C (%)	3.06	−0.15
LOI 750 °C (%)	–	0.83
LOI 550 °C (%)	1.07	–

2.1.2. Mix design

The mix designs are based on the guidelines in Specifications and Guidelines for Self-Compacting Concrete [26] and the proportions are reported in Table 3. All mixtures have a total cement content of 440 kg/m^3 and a water-to-cementing materials (w/cm) ratio of 0.4. The cementing material is a binary blend of 75% type GU cement and 25% GGBFS, which is the maximum cement replacement percentage permitted by the MTO for structural elements exposed to freezing and thawing in the presence of de-icing salts [27]. The coarse aggregate content for all mixes is 895 kg/m^3.

The mix variables in this study are the coarse aggregate gradation (A and B), level of air entrainment (non-air entrained and $7 \pm 1\%$ entrained air) and use of viscosity modifying agent (used and not used). Although non-air entrained concrete would not be specified for outdoor applications in Ontario, it was studied for two reasons: to represent the extreme case of under-air entrained concrete and to assess the effect of segregation measurements over a range of durability performance. Furthermore, a constant superplasticizer dosage was used for all mixes to intentionally yield concrete with a range of strong and poor segregation resistance.

2.1.3. Mixing, casting and curing

All mixtures were prepared in 65 L batches in an 81 L capacity pan mixer. The mixing sequence was the same for all mixtures as reported in Panesar and Shindman [28]:

i. The fine aggregate, coarse aggregate and 85% of the mixing water were mixed for 60 s. The air entraining agent, if used, was diluted in this first water addition.
ii. The cementing materials were then added and mixed for 3 min, with the remaining water being added while the mixer was running.
iii. The superplasticizer was added and the concrete was mixed for an additional 7 min.
iv. The viscosity modifying agent, when used, was added 30 s after the superplasticizer.

Table 3
Mix design proportions.

	GU cement	GGBFS	Fine aggregate	Coarse aggregate	Water	SP	AEA	VMA
	kg/m^3					mL/100 kg		
Mix1	330	110	895	895	176	700	0	0
Mix2	330	110	895	895	176	700	0	200
Mix3	330	110	760	895	176	700	5	0
Mix4	330	110	760	895	176	700	5	200
Mix5	330	110	895	895	176	700	0	0
Mix6	330	110	895	895	176	700	0	200
Mix7	330	110	760	895	176	700	5	0
Mix8	330	110	760	895	176	700	5	200

The aggregate preparation, material measurement, specimen casting and testing were consistent for all batches of concrete. The plastic air content was measured in accordance with MTO LS-436 [29] based on the pressure method. Following confirmation that the target air content was achieved (i.e. 7 ± 1% for air entrained mixtures) the plastic property measurements were conducted in the same order for all eight mixtures: slump flow (VSI), plastic air content, column segregation and, lastly, the V-funnel (t_5–t_0). The test specimens were cast upon the completion of plastic property testing. In order to minimize the effect of heterogeneities of the concrete in the mixer, prior to casting each set of specimens, the concrete in the mixer was turned by hand using a scoop. All specimens were demoulded at 24 h. The cylinders for compressive strength and rapid chloride permeability testing were cured at 23 ± 2 °C and 100% relative humidity until testing. Test specimens for sorptivity and salt scaling were cured at 23 ± 2 °C and 100% relative humidity for 14 days followed by 14 days at 23 ± 2 °C and 50 ± 5% relative humidity. Specimens for freeze–thaw testing were cured in saturated limewater for 14 days at 23 ± 2 °C.

2.2. Test procedures

2.2.1. Segregation resistance

This study evaluates the segregation resistance of SCC by the column segregation test [30,31], the visual stability index (VSI) [32,33] and the V-funnel (t_5–t_0) test [34]. It should be noted that although each of the plastic property tests is conducted in accordance with MTO specifications, each MTO guideline is based on or refers to ASTM standards or EFNARC guidelines. Specifically, MTO LS-442 [31] refers directly to ASTM C1610 [30] for the static segregation of SCC using the column technique. The MTO LS-438 [33] is the same as ASTM C1611 [32] to evaluate the slump flow and VSI, and MTO LS-441 [34] is similar to the V-funnel test specified in EFNARC [20]. The mortar band thickness determined using digital image analysis is also used to indicate segregation. The procedural development, consisting of sample preparation, scanning and mortar band analysis is involved and so is detailed in Section 3.

Segregation resistance evaluated by the VSI is assessed by observing the periphery of the concrete after the slump flow test. VSI ratings range from zero to 3 and are used to rate the SCC based on the descriptions stated in Table 4 [35]. This method evaluates segregation qualitatively and relies on the experience and judgment of the individual conducting the test. The maximum VSI rating permitted in accordance with the MTO special provisions (SP) document MTO-SP-SCC [36] is 1.5.

Table 4
Visual stability index rating scale [35].

Rating	description
0	No evidence of segregation in the slump flow patty, mixer drum or sampling wheelbarrow.
0.5	No mortar halo or aggregate pile in the slump flow patty, but very slight evidence of bleeding or air popping on the surface of the SCC in the mixer drum or sampling wheelbarrow.
1.	No mortar halo in the slump flow patty, but some slight bleeding on the surface of the concrete in the mixer drum and/or wheelbarrow.
1.5	Just noticeable mortar halo and/or a just noticeable aggregate pile in the slump flow patty and noticeable bleeding in the mixer drum and sampling wheelbarrow.
2	Slight mortar halo (<10 mm) in slump flow patty and noticeable layer of mortar on the surface of the testing concrete in the mixer drum and wheelbarrow.
3	Clearly segregating by evidence of large mortar halo (>10 mm) and thick layer of mortar and/or bleed water on concrete surface in mixer or wheelbarrow.

The column segregation test method evaluates static stability, however, it should be noted that some dynamic segregation may occur when filling the 200 mm diameter × 660 mm high column with concrete. After letting the concrete rest in the column for 15 min, the concrete in the top and bottom sections of the column are washed over a 4.75 mm (No. 4) sieve. The coarse aggregate is then dried and weighed, and the column segregation (*seg*) is calculated according to Eq. (1), where m_{top} and m_{bot} represent the mass of coarse aggregate from the top and bottom sections of the column, respectively. The acceptance limit set by MTO-SP-SCC [36] and Canadian Standards Association (CSA) A23.1 [21] is a maximum of 10%. EFNARC [20] does not specify limits for acceptable column segregation.

$$seg = 2\frac{m_{bot} - m_{top}}{m_{bot} + m_{top}} \quad (1)$$

The V-funnel test is used to evaluate the filling ability and viscosity of SCC by measuring the time for the concrete to empty the V-funnel once the gate is opened [34]. By comparing t_5 to t_0, where t_x is the V-funnel time after the concrete has been allowed to rest in the V-funnel for *x* minutes, the dynamic stability can also be evaluated [26]. The acceptance criterion for the V-funnel (t_5–t_0) measurement is a maximum of 3 s in accordance with MTO-SP-SCC [36]. It should be noted that this method does assess plastic viscosity but does not give a quantitative evaluation of segregation and neither EFNARC [20] nor CSA A23.1 [21] specify acceptance criteria for the V-funnel (t_5–t_0) test.

2.2.2. Mechanical properties

Compressive strength was evaluated in accordance with ASTM C39 [37] as specified in MTO LS-437 [38]. Compressive strength was measured at days 1, 3, 7, 28 and 56 as reported in [28]. For each mix at each age, three cylinders, 100 mm diameter × 200 mm in high, were tested.

2.2.3. Transport properties

Rapid chloride permeability was measured in accordance with ASTM C1202 [39] on three specimens cut from one cylinder, 100 mm diameter × 200 mm height. The rapid chloride permeability test was conducted at days 28 and 56. The tested surfaces were at nominal depths of 40, 90 and 140 mm from the top surface of the cylinder.

Sorptivity was measured in accordance with ASTM C1585 [40]. Cylinders, 100 mm diameter × 200 mm in height, were cut to retrieve pucks 50 mm high. The puck with the bottom surface (formed surface) of the cylinder and the top (struck-off) surface were tested. Two samples per mix per surface type (top or bottom) were tested. As per the specifications, test specimens were cured for 14 days at 100% relative humidity followed by 14 days at 50% relative humidity. The specimens were then conditioned in a chamber at 50 °C and 80% relative humidity for three days, followed by 15 days in a sealed container at room temperature. The initial (6 h) sorptivity measurements were carried out at day 43. The cylinder perimeter was sealed using two layers of electrical tape. The samples were then placed in contact with the sorbing solution, water, while resting on a thin wire mesh to allow free access of the sorbing fluid at the concrete surface. The absorption (mm) was calculated by measuring the change of the specimen mass with time from 1 min to 6 h which is a function of the density of the sorbing fluid and the cross sectional area in contact with the fluid. The sorptivity or initial rate of absorption ($mm/s^{0.5}$) is:

$$I = S\sqrt{t} + b \quad (2)$$

where *S* is the sorptivity or the initial rate of absorption ($mm/s^{0.5}$) determined from least squares linear regression and *b* is the corresponding constant value in accordance with ASTM C1585-04 [40].

2.2.4. Durability properties

Freeze–thaw resistance was determined in accordance with ASTM C666 Procedure A [41]. The test commenced at 14 days and the samples were subjected to 300 freeze–thaw cycles. At intervals of 36 cycles, the specimens were removed from the apparatus and the fundamental transverse frequency was measured to determine the relative dynamic modulus of elasticity of the specimens. Two specimens per mix design were tested.

The laboratory de-icer salt scaling test determines the resistance of a horizontal concrete surface to scaling when exposed to freeze–thaw cycles in the presence of de-icing solution. Testing was conducted in accordance with MTO LS-412 [42], which is similar to ASTM C672 [43] except that a 3% NaCl de-icer solution is used instead of 4% $CaCl_2$. It should be noted that, during casting of the specimens, the top surface was not finished but was only struck off to remove excess material. The scaling resistance was quantitatively measured by weighing the dry mass of the flaked-off concrete after every five freeze–thaw cycles, at which time the salt solution was washed off the concrete surface and replaced. The mass of the scaled residue divided by the specimen's area exposed to de-icer solution is defined as the mass loss and is calculated to the nearest 0.01 kg/m^2. A salt scaling value of 0.8 kg/m^2 is the specified acceptance limit in accordance with OPSS 1351 [44]. In this study, if the average salt scaling value based on two slabs of the same mix design exceeded 0.8 kg/m^2, the test was terminated prior to 50 cycles. After the top surface was tested, the slabs were turned over and the bottom surface was tested.

3. Development of procedure for digital image analysis

The objective of using digital image analysis is to quantify the average thickness of the mortar band layer at the top and bottom surfaces of a 100 mm diameter × 200 mm high concrete cylinder. In this analysis, mortar is defined as having a maximum aggregate size of 4 mm. It is expected that the thicker the mortar band at the top of the cylinder, the greater severity of segregation owing to coarse aggregate settlement. This is supported by the hardened visual stability ratings summarized in Table 5 as reported by Fang and Labi [45]. The rating system indicates that a slight mortar band layer (<25 mm) and a thicker mortar band layer (>25 mm) are unstable [45].

In this study, the mortar band thickness is defined as the distance from the top or bottom edge of the cylinder to the first encounter with coarse aggregate. Quantification of the mortar band using digital image analysis software requires that the scanned image have an acceptable sharpness, brightness and contrast in order for the software to distinguish between the concrete's paste and aggregate phases. The coarse aggregate used in this study exhibits similar color and brightness in comparison to the cement paste. To create contrast, phenolphthalein was chosen to color the paste because its transition range is close to the pH of cement paste. The effectiveness of phenolphthalein to create brightness contrast was assessed by evaluating three sample preparation variables:

i. Surface finish: saw cut or polished
ii. Drying method prior to application of phenolphthalein: wipe dry, pat dry or blow dry
iii. Surface wetness: wet, saturated surface dry (SSD) or air dried

The best quality of paste–aggregate contrast was achieved on a saw cut surface, where the surface is patted dry until a SSD condition is achieved. After phenolphthalein application, additional sample preparation factors were examined in order to create uniform contrast and enhance the brightness of the scanned images. Four sample preparation approaches were conducted which entailed examination of: the effect of minimizing surface dust particles; optimizing the amount of phenolphthalein solution on the surface; and determination of the effect of applying a surface coating.

First approach: Cylinders were saw cut in half lengthwise, rinsed with water, patted dry to a SSD condition and then sprayed with phenolphthalein. After 16 h at room temperature, the specimens were scanned and the images are shown in Fig. 1a. A key problem with the images is the inconsistent brightness of the pink phenolphthalein color. Additionally, many pieces of coarse aggregate were stained pink, making it impossible for the software to differentiate between aggregate and paste.

Second approach: Specimens were saw cut in half lengthwise, and then the cut surface was washed with a pressure washer. The pressure washer was used to remove dust particles and saw cuttings that may have been situated within the pores of the paste and aggregate. The cut and washed surface was then patted dry to a SSD condition and sprayed with phenolphthalein. After resting at room temperature for 16 h, excess phenolphthalein was rinsed off the surface of the concrete with water. The specimens were then blown dry with compressed air and scanned. Fig. 1b shows an improved consistency of the color brightness and fewer stained pieces of coarse aggregate in comparison to the first approach, shown in Fig. 1a. However, difficulty in determining the paste–aggregate boundary was still encountered due to the presence of some aggregate stained pink.

Third approach: The sample was saw cut in half lengthwise, rinsed with water, patted dry to a SSD condition and then sprayed with phenolphthalein. Once the paste had changed color, the specimens were rinsed with a gentle spray of water to remove the excess phenolphthalein. Once the rinse water running off the specimen surface was no longer pink, the specimens remained at room temperature for 16 h prior to scanning, as shown in Fig. 1c. This approach resulted in a uniform paste color and minimal aggregate staining; however, the image is not as bright as that from the previous approach.

The first, second and third sample preparation approaches focused on thorough cleaning of the concrete surface before spraying. However, the scanned images still lacked the desired quality of contrast. A major impediment to effective and accurate characterization using the imaging software is lack of clarity and sharpness of the paste–aggregate interface.

Fourth approach: Samples were saw cut lengthwise, rinsed with water, patted dry to a SSD condition, sprayed with phenolphthalein and rinsed with a gentle spray of water to remove excess phenolphthalein. After 16 h, the phenolphthalein-treated surface was coated with a 0.5 mm layer of petroleum jelly for which was wiped off with paper towels after 5 min, leaving only a thin film of the petroleum jelly on the concrete surface. The samples were then scanned.

Table 5
Hardened concrete visual stability index [45].

Rating	Description
0- Stable	No mortar layer at the top of the cut plane and no variance in size and percent area of coarse aggregate distribution from top to bottom.
1- Stable	No mortar layer at the top of the cut plane but slight variance in size and percent area of coarse aggregate distribution from top to bottom.
2- Unstable	Slight mortar layer, less than 25 mm thick at the top of the cut plane and distinct variance in size and percent area of coarse aggregate distribution from top to bottom.
3- Unstable	Clearly segregated as evidenced by a mortar layer greater than 25 mm thick and or considerable variance in size and percent area of coarse aggregate distribution from top to bottom.

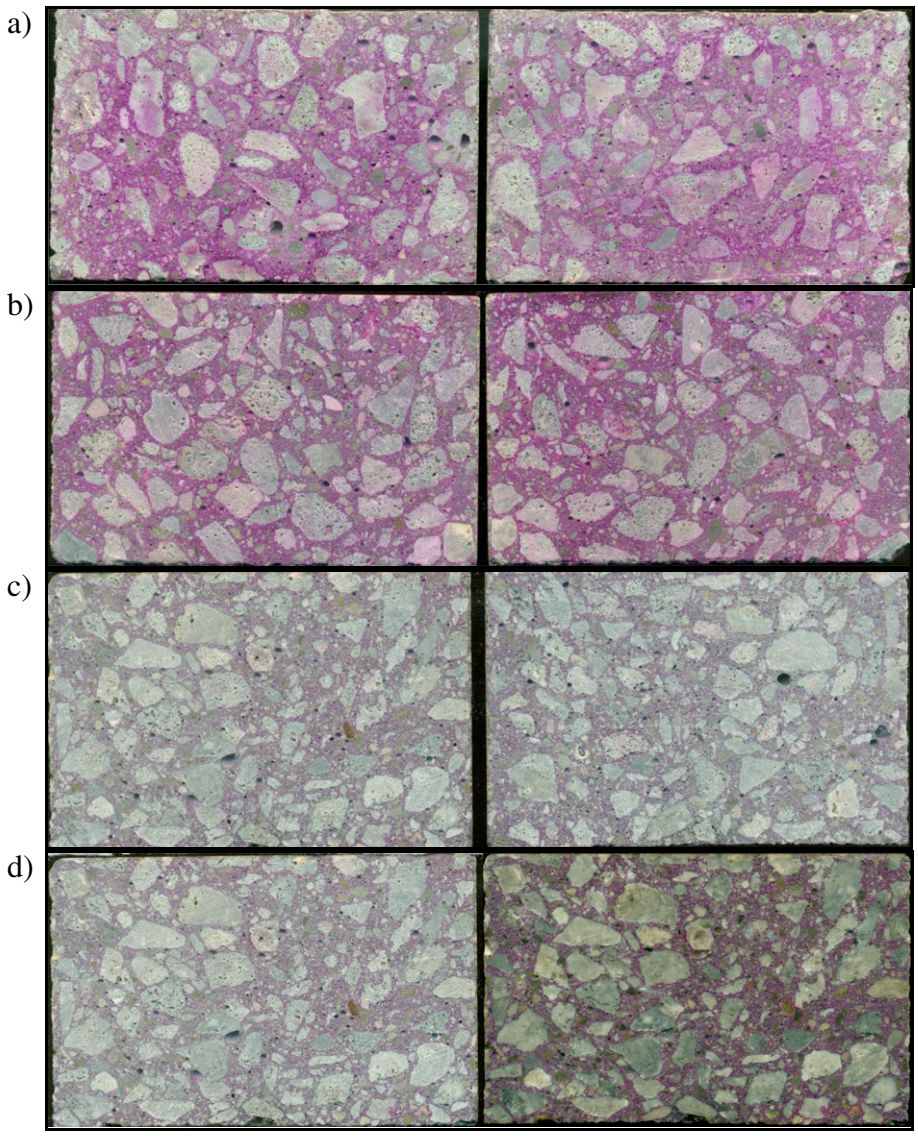

Fig. 1. The effect of different sample preparation techniques on brightness and contrast between aggregate and paste phases. a) First approach, b) Second approach, c) Third approach, d) Fourth approach—left hand side: no petroleum jelly coating, right hand side: with petroleum jelly coating.

Fig. 1d shows a comparison of the contrast without any coating (left hand side image) and with petroleum jelly coating (right hand side image). The application of the coating resulted in an enhanced clarity and contrast by making the aggregate appear lighter and the paste appear darker.

The following summarizes the steps used for sample preparation, scanning and digital image analysis.

Concrete sample preparation procedure

i. Cut the concrete specimen to expose a fresh face.
ii. Rinse the cut face with water to remove saw cuttings. This can be done using any source of running water.
iii. Pat the surface dry to remove any free water, leaving the concrete in a SSD condition.
iv. Spray the cut surface of the concrete with 1% phenolphthalein solution.
v. Once the paste phase changes to a pink color, rinse the concrete with tap water to remove excess phenolphthalein. Rinse until the runoff water is clear.
vi. Allow the concrete to air dry at room temperature for at least 16 h. Compressed air may be used to quickly dry the concrete if waiting until the next day is not desired.
vii. Apply a thin coat of petroleum jelly to the sprayed surface and remove the excess with a paper towel. Removing the excess petroleum jelly reduces the reflectivity of the prepared surface, improving the quality of the scanned image. This step can be done any time after step vi.

Scanning procedure

viii. Create a digital image of the concrete using a flatbed scanner. To protect the scanner, a piece of acetate (transparency) should be placed on the scanning glass as a sacrificial surface.
ix. To ensure sufficient edge detail in the images, the concrete samples should be scanned at high resolution. Scanning the concrete at 600 pixels per 2.54 cm provides sufficient detail while keeping the 16 bit tiff file size below 100 Mb.
x. To ensure accurate measurements, the samples are scanned with a scale bar, as shown in Fig. 2a.

Digital image analysis procedure

The digital image analysis software ImageJ (available from www.rsbweb.nih.gov/ij) was used to quantify the mortar band thickness. The following steps were used to analyze the image and compute the mortar band thickness.

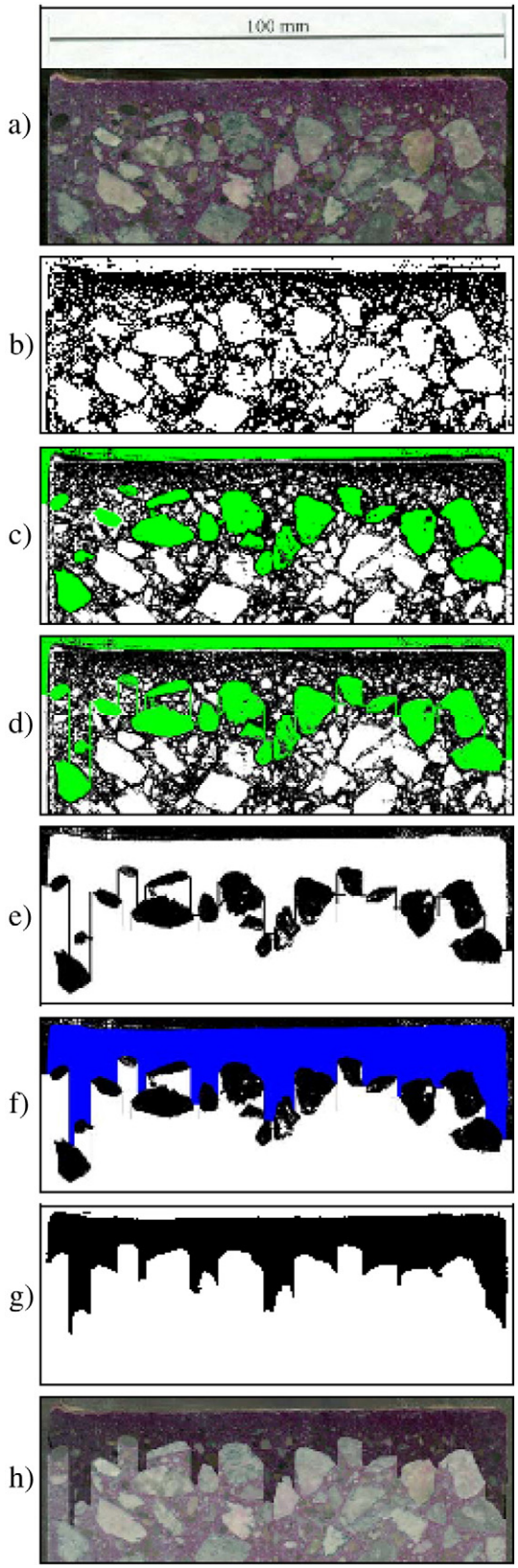

Fig. 2. Illustrations of digital image analysis procedure: a) scanned image with scale; b) threshold image (black—paste, white—aggregate); c) identify top most layer of coarse aggregate; d) define mortar band–concrete boundary; e) threshold image to image the boundary in black; f) fill in mortar band with blue; g) threshold image (black—mortar band, white—concrete); h) mortar band image (g) superimposed with original scan (a).

xi. Threshold the image to separate the aggregate (white) and paste (black) phases as shown in Fig. 2b.
xii. Divide the image into two parts, using the topmost piece of coarse aggregate as the dividing line. Coarse aggregate is considered to be any piece of aggregate that will not fit into a 4 mm diameter circle as shown Fig. 2c.
xiii. Make the dividing line continuous by connecting the coarse aggregate particles with vertical lines. Coarse aggregate particles that are adjacent should be connected with a horizontal line as indicated in Fig. 2d. Two coarse aggregate particles are considered adjacent if the distance between them is less than 2 mm.
xiv. Threshold the image to separate the dividing line (black) from the rest of the image (white) as illustrated in Fig. 2e.
xv. Fill in the mortar band that is shown in blue in Fig. 2f, and then threshold the image to isolate the mortar band as illustrated in Fig. 2g.
xvi. Clean the image to correct threshold errors both manually and by using the commands in the 'Process > Binary' submenu. Fig. 2h illustrates the final image overlaid on the original image.
xvii. Analyze the modified image using the 'analyze particles' command.
xviii. Divide the mortar band into sections 0.5 mm wide and run the 'analyze particles' command again to determine statistics. The output of this analysis is the area and width of each piece of the mortar band.
xix. Calculate the average mortar band thickness by dividing the area by the scanned sample width, using the output from step xvii.

4. Results and discussion

4.1. Segregation resistance

Table 6 summarizes the segregation test results. For the eight mix designs, the column segregation values range from 1.9 to 11.5%, the VSI ranges from 0.5 to 3, and the V-funnel time differences (t_5–t_0) range from 0 to 8.5 seconds. For all tests, the results span good, borderline and poor segregation resistance based on the MTO-SP-SCC [36] acceptance limits discussed in Section 2.2.1. Overall, the results show that by comparing mixtures with VMA (mixtures 2, 4, 6, 8) to mixtures without VMA (mixtures 1, 3, 5 and 7), there is no consistent effect on the segregation. For example, irrespective of whether VMA was used or not, mixtures containing entrained air had VSI equal to or exceeding the 1.5 limit, and those without air entrainment had VSI ratings of or below 1.5. Similar trends were observed for the column segregation and V-funnel test indicating that the VMA did not affect the segregation test measurements. The presence of VMA did not affect the hardened properties of SCC either. This is likely attributed to the fact that all of the other material proportions were held constant including the superplasticizer dosage [46].

Table 6 also presents the mortar band thicknesses for the top and bottom surfaces of a cylinder for each mix design. As expected, the

Table 6
Segregation measurements and mortar band thickness.

	Visual stability index (VSI)	Column segregation (%)	V-funnel t_5–t_0 (s)	Mortar band thickness (mm)	
				Top	Bottom
Mix1	1.5	6.0	0.5	6.0	5.1
Mix2	1.0	5.1	3.5	5.6	5.5
Mix3	2.0	10.0	5.5	7.3	3.7
Mix4	2.0	7.7	7.0	10.7	4.5
Mix5	1.5	10.8	3.0	8.5	4.8
Mix6	0.5	1.9	0.0	6.8	4.3
Mix7	1.5	9.4	8.5	10.1	3.8
Mix8	3.0	11.5	3.0	9.3	3.6

range of mortar band thicknesses of the bottom surface is narrow, from 3.6 to 5.5 mm. In contrast, the range of mortar band measurements is larger for the top surface, ranging from 5.6 to 10.7 mm.

Fig. 3 is plotted in order to evaluate the correlation between the mortar band thickness at the top surface and the segregation measured using the column method, VSI and V-funnel (t_5–t_0). The normalized segregation index shown in Fig. 3 was calculated by dividing the test measurement by the MTO-SP-SCC [36] acceptance limit. A normalized segregation index of 1.0 for the column, VSI, and V-funnel tests indicates that the segregation measurement is equal to the acceptance limit of 10%, 1.5, and 3 seconds, respectively. A normalized segregation index less than 1.0 indicates that the segregation measurement is below the maximum allowable limit, and a normalized segregation index greater than 1.0 indicates that the segregation exceeds the acceptable limit.

The normalized segregation index plotted against the mortar band thickness in Fig. 3 reveals that although there is scatter in the measured data, the thickness of the mortar band is greater at high segregation values in comparison to low segregation values for all three segregation tests. In addition, for the column segregation, VSI and V-funnel (t_5–t_0) measurements, a range of mortar band thicknesses is observed closely surrounding the normalized segregation index of 1.0. Thus, the mortar band measurements for concrete that exhibits borderline acceptable segregation with respect to specified acceptance criteria may be similar to SCC which exhibits segregation measurements well below or above the acceptance limits. For instance, with column segregation values close to 10% and a VSI of approximately 1.5, the mortar band thickness ranges from approximately 6 to 11 mm. At normalized segregation index values less than 0.7, the mortar band thickness ranges from 5 to 7 mm. In contrast, at normalized segregation index values greater than 1.3 the mortar band thickness is as large as approximately 11 mm.

4.1.1. Effect of segregation on compressive strength

Fig. 4a, b, and c shows the mean compressive strength at days 1, 3, 7, 28 and 56 plotted with segregation measured by the column technique, VSI and V-funnel (t_5–t_0), respectively. The results reveal that regardless of which segregation test is used, the compressive strength is not adversely affected by poor segregation performance and is also supported by [47]. For example, the compressive strengths for all mixtures range from 20–25 MPa at day 1 to 62–67 MPa at day 56 irrespective of the segregation performance.

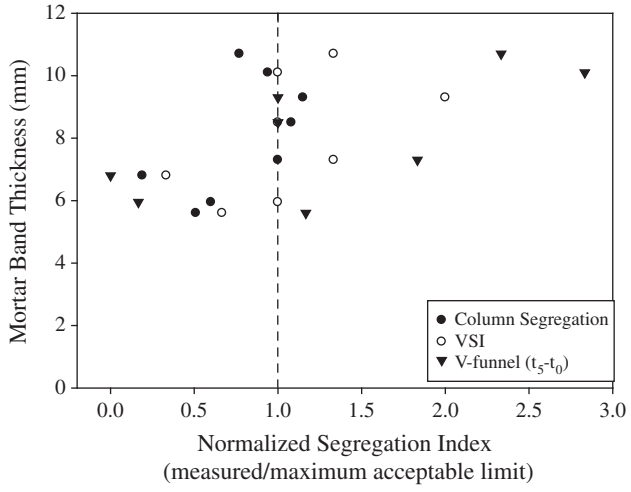

Fig. 3. The correlation between the average mortar band thickness of the top surface and normalized segregation index.

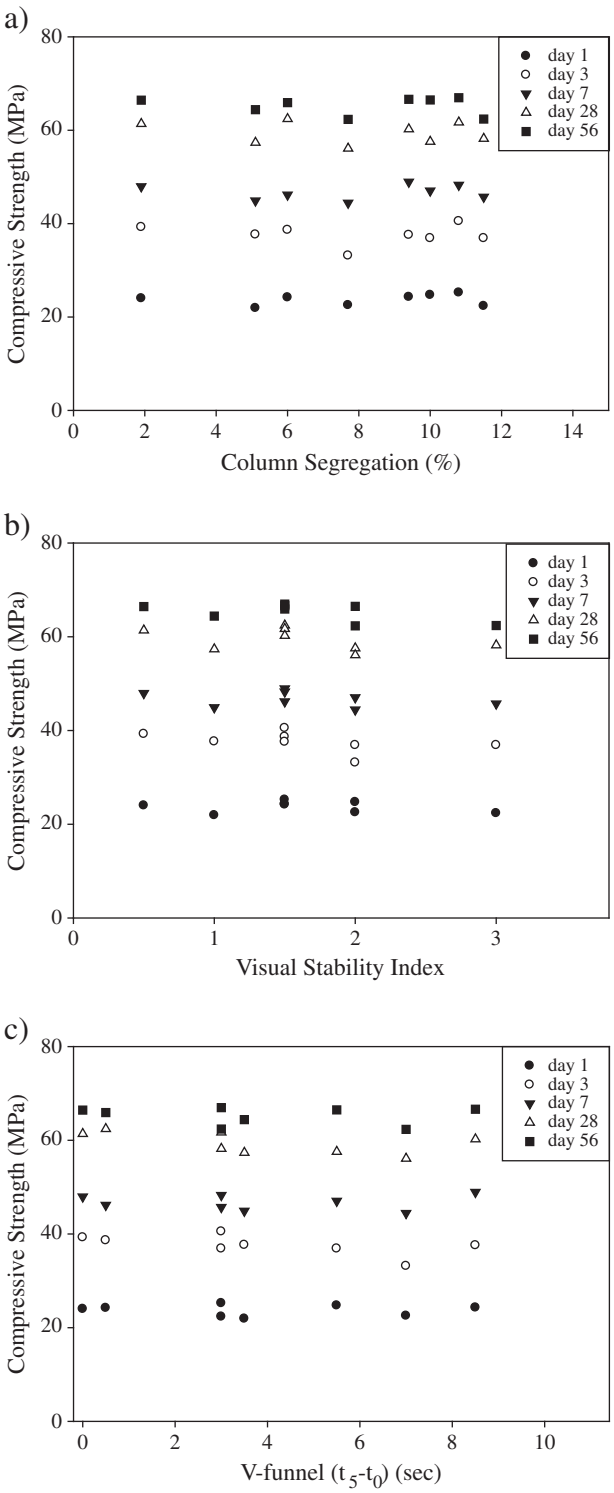

Fig. 4. The correlation between mean compressive strength and segregation measured by: a) column method, b) VSI, and c) V-funnel (t_5–t_0).

4.1.2. Effect of segregation on transport properties

Fig. 5a, b and c shows that all rapid chloride permeability measurements are low in accordance with the MTO-SP-SCC [36] limit of 2500 C. There is no observable correlation between the rapid chloride permeability and segregation resistance based on the column segregation method, VSI or V-funnel (t_5–t_0) measurements.

Table 7 summarizes the initial sorptivity coefficients taken at the top and bottom surfaces of the test cylinder. Comparing mixtures with and without the use of VMA did not have any effect on the sorptivity or the

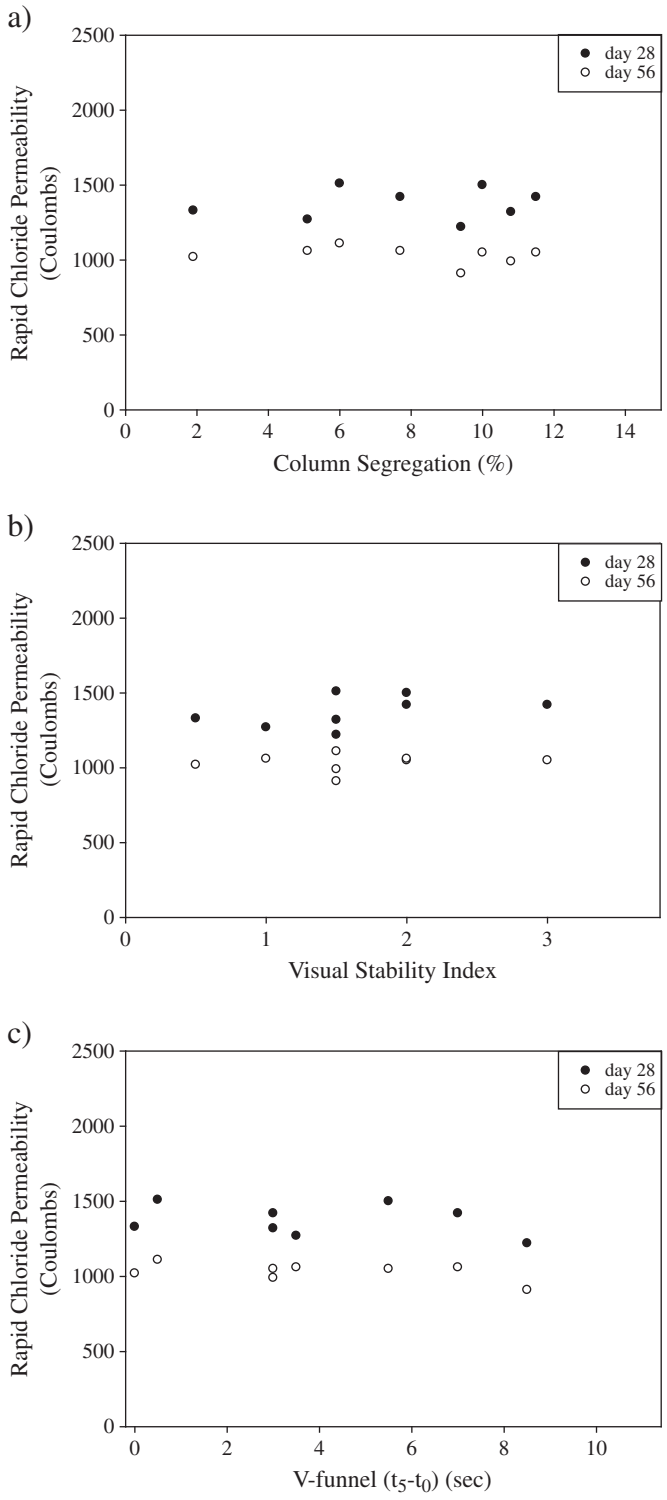

Fig. 5. The correlation between rapid chloride permeability and segregation measured by: a) column method, b) VSI, and c) V-funnel (t_5–t_0).

other hardened properties reported in Table 7. However, for both surfaces, the initial sorptivity coefficient of the air entrained mixtures (# 3, 4, 7 and 8) is higher than the corresponding non-air entrained mixtures (#1, 2, 5 and 6). For all mixtures, the sorptivity of the bottom (formed) surface is less than the corresponding top surface. This result is expected owing to differences in composition, quality, and microstructural properties of concrete, which are known to be different at the cover in comparison to the core or bottom surface [48,49]. In this

Table 7
Transport and durability properties.

		Initial sorptivity ($\times 10^{-4}$ mm/s$^{0.5}$)		Salt scaling mass loss (kg/m^2)		Freeze/thaw durability factor (%)
		Top	Bottom	Top	Bottom	
Mix1 (3.6% air content)	1	26.8	18.7	1.34	0.43	15
	2	15.8	12.6	0.85	0.42	12
	Mean	21.3	15.6	1.10	0.43	14
	Cycles[a]	N.A.	N.A.	25	50	300
Mix2 (3.5% air content)	1	18.7	12.6	1.23	0.75	21
	2	17.6	15.7	1.11	1.01	44
	Mean	18.1	14.1	1.17	0.88	33
	Cycles	N.A.	N.A.	20	50	300
Mix3 (7.2% air content)	1	41.5	30.4	0.37	0.05	64
	2	40.0	24.2	1.15	0.12	77
	Mean	40.7	27.3	0.76	0.08	71
	Cycles	N.A.	N.A.	50	50	300
Mix4 (8.0% air content)	1	37.5	27.1	0.42	0.18	96
	2	34.7	27.7	0.36	0.16	94
	Mean	36.1	27.4	0.39	0.17	95
	Cycles	N.A.	N.A.	50	50	300
Mix5 (3.8% air content)	1	34.1	21.3	1.60	0.10	24
	2	35.4	23.2	1.07	0.14	23
	Mean	34.7	22.2	1.33	0.12	24
	Cycles	N.A.	N.A.	15	50	300
Mix6 (4.3% air content)	1	22.3	20.3	0.83	0.99	30
	2	25.8	19.2	2.46	0.64	35
	Mean	24.0	19.8	1.65	0.81	33
	Cycles	N.A.	N.A.	20	50	300
Mix7 (6.0% air content)	1	25.1	19.3	0.62	0.06	72
	2	28.2	17.9	0.43	0.09	54
	Mean	26.6	18.6	0.52	0.07	63
	Cycles	N.A.	N.A.	50	50	300
Mix8 (6.2% air content)	1	46.9	19.4	0.89	0.08	93
	2	38.5	23.8	1.12	0.08	94
	Mean	42.7	21.6	1.01	0.08	94
	Cycles	N.A.	N.A.	50	50	300

[a] 'Cycles' refers to the number of freeze–thaw cycles the specimen underwent.

study, the range in sorptivity coefficient of the bottom surface compared to the top surface for the same cylinder is broad. The bottom surface is not expected to be affected by surface settlement or bleeding and this is reflected in the sorption values, which range from 14.1 to 27.4×10^{-4}mm/$\sqrt{\text{sec}}$. In contrast, the value and range of sorptivity coefficients are larger for the top surface which, based on average values, ranges from 18.1 to 42.7×10^{-4}mm/$\sqrt{\text{sec}}$. Discriminating between the effect of segregation, sorptivity and durability of the top surface in comparison to the bottom surface is of particular importance in context with real world applications. For cast in place structures, the top surface is commonly exposed to the environment, consisting of moisture and ions and so is vulnerable to damage.

The correlation between initial sorptivity and column segregation and VSI reveals an increase in initial sorptivity of the concrete's top surface with increasing segregation, as presented in Fig. 6a and b, respectively, but no correlation with V-funnel (t_5–t_0) measurements as shown in Fig. 6c. The correlation between the increasing initial sorptivity of the top surface with greater column segregation and VSI rating is attributed to the mortar layer with a higher volume of capillary pores. This is supported by Fig. 7, which shows a general

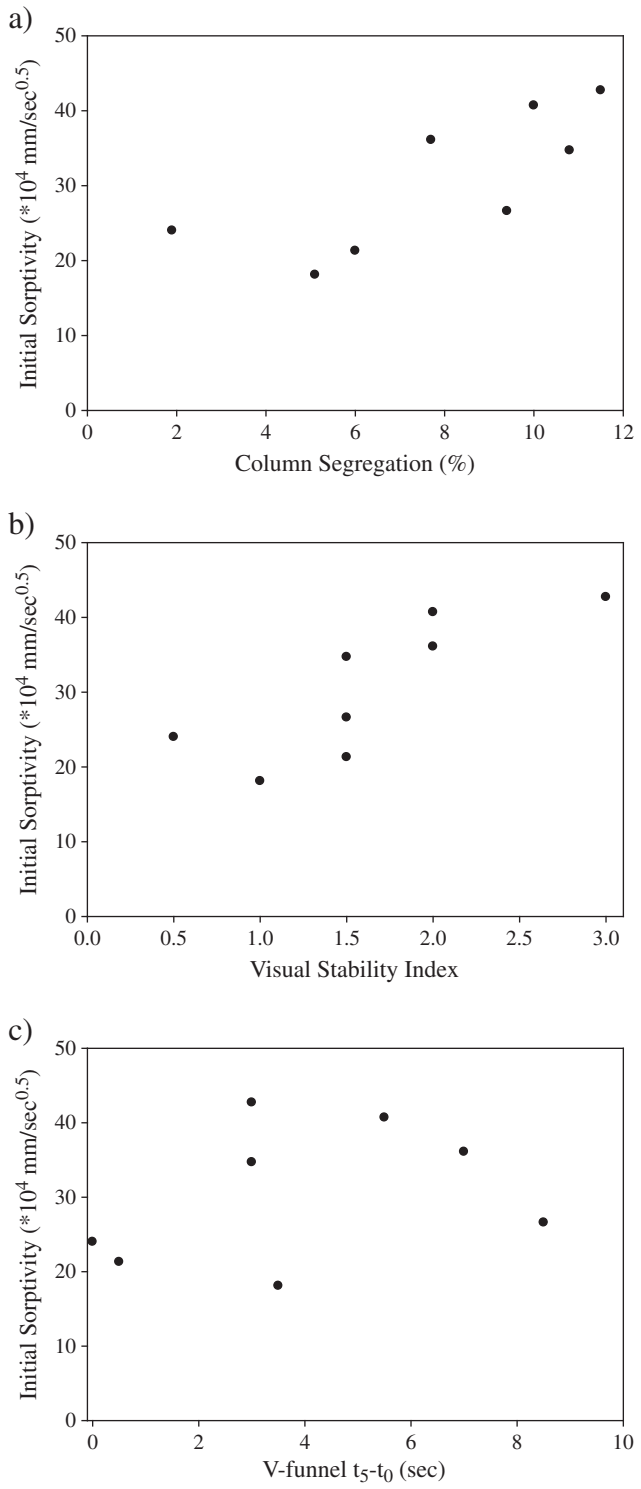

Fig. 6. The correlation between initial sorptivity of the top surface and segregation measured by: a) column method, b) VSI, and c) V-funnel (t_5–t_0).

increasing trend between the initial sorptivity and mortar band thickness for both the air entrained and non-air entrained mixtures.

4.1.3. Effect of segregation on durability performance

For conventional concrete, it is well established that increased air content is associated with improved freeze–thaw performance and salt scaling resistance [50]. This relationship also holds for SCC and is supported by other studies [16,51–53]. As shown in Table 7 and Fig. 8, both freeze–thaw and salt scaling resistance of SCC improve

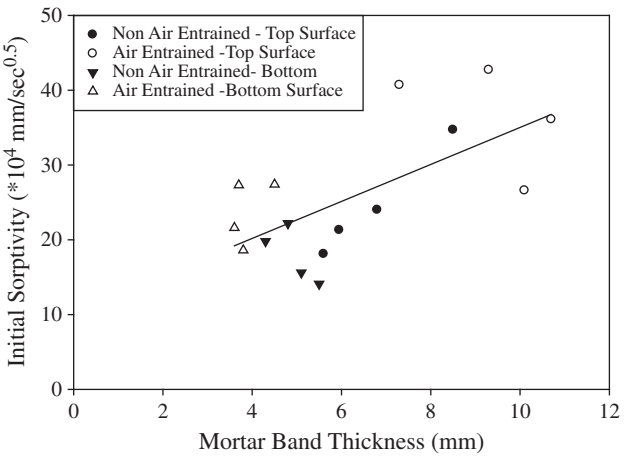

Fig. 7. Correlation between initial sorptivity and mortar band thickness.

significantly with increased plastic air content. Air entrainment increases the freeze–thaw resistance approximately three-fold compared to the non-air entrained mixes. After 300 rapid freeze–thaw cycles, all of the air entrained prisms were physically intact, while three of the eight non-air entrained prisms had disintegrated and the other five non-air entrained prisms were visibly deteriorated.

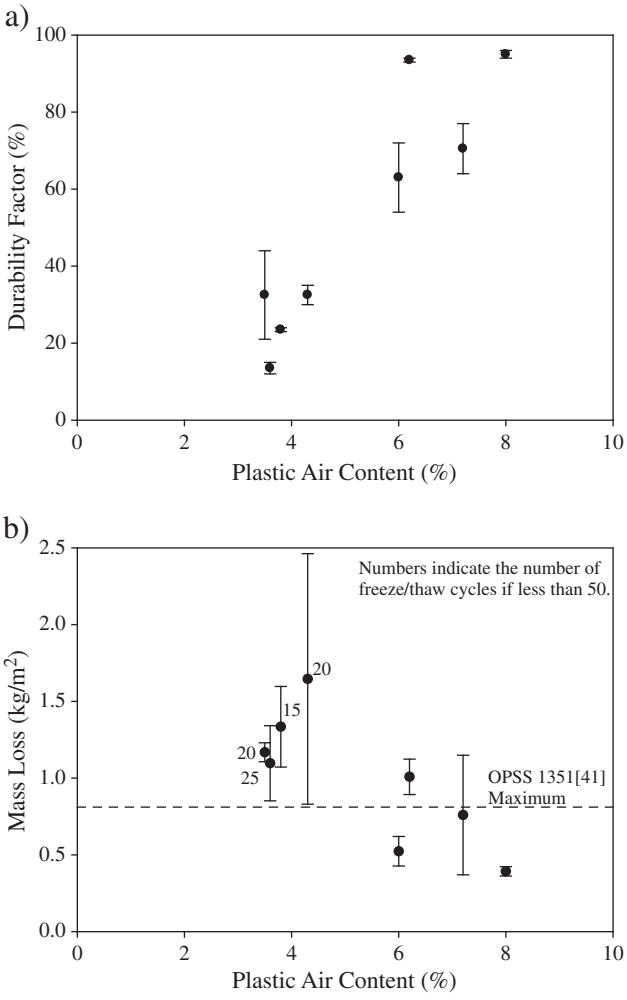

Fig. 8. The influence of plastic air content on a) freeze–thaw durability factor, and b) de-icer salt scaling mass loss.

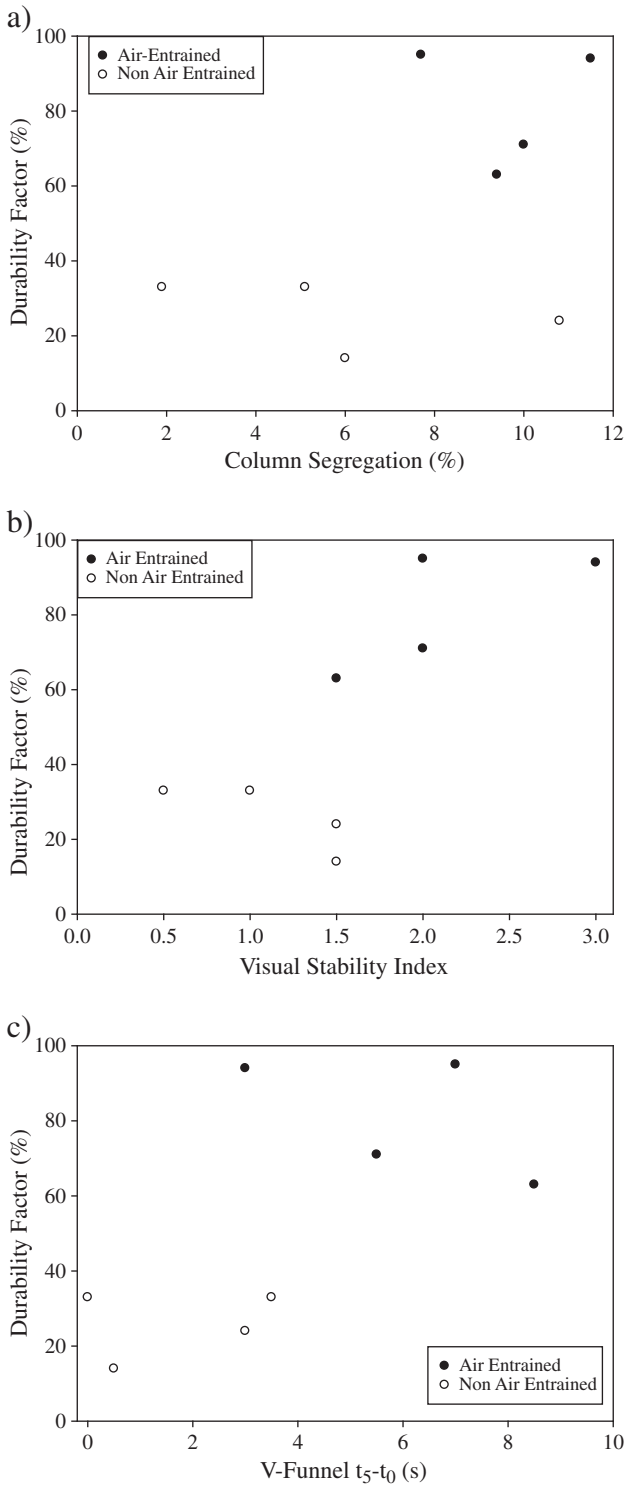

Fig. 9. The correlation between freeze–thaw durability and segregation measured by: a) column method, b) VSI, and c) V-funnel (t_5–t_0).

Fig. 9 presents the impact of segregation on the freeze–thaw durability factor. Although at a first glance, the plotted data shows that the higher durability corresponds to greater segregation, the effect of air entrainment should be noted. All of the air entrained mixtures exhibited a relatively higher freeze–thaw resistance but poorer segregation resistance in accordance with the column technique, VSI and V-funnel (t_5–t_0) tests. These results can be explained by examining the interplay between air entrainment, rheological parameters, and segregation. Although evaluation of the rheological parameters was not conducted in this study, data from reported literature is used to explain some of the observations. Few studies have reported direct correlations between the rheological parameters (yield stress and plastic viscosity) and plastic properties, specifically segregation resistance of SCC. Koehler and Fowler [54] reported that no single rheological parameter was directly correlated to segregation resistance evaluated by the column segregation test. Although they found that increasing the static or dynamic yield stress resulted in increased segregation resistance, their experimental data did exhibit a relatively high degree of scatter. By examining combinations of rheological parameters, Koehler and Fowler [54] reported that to minimize segregation the plastic viscosity should increase as the dynamic yield stress decreases. Koehler [55] and Zerbino et al. [56] reported that low plastic viscosity would result in poor stability based on the column segregation method V-funnel times, respectively.

The effect of air entrainment in SCC has been reported to decrease the plastic viscosity and result in a minimal decrease or a mixed effect on the yield stress [2]. The effect of air entrainment in SCC was observed to lead to a decrease in plastic viscosity and an increase in V-funnel times [57]. The relatively longer V-funnel flow times for unstable mixtures was partially due to aggregate interaction in the vicinity of the V-funnel outlet [57]. Consistent with the literature, this study reveals that air entrained SCC exhibits poorer segregation resistance in comparison to non-air entrained mixtures. Even though air entrained mixtures experience poorer segregation; they are more resistant to freeze–thaw damage in comparison to non-air entrained mixtures which have been shown to segregate relatively less. This indicates that the freeze–thaw performance of SCC is controlled by air content over segregation, which is strongly linked to lower plastic viscosity.

The salt scaling results shown in Table 7 show a stronger resistance to scaling of the bottom surface in comparison to the top surface. This observation is supported by many research studies that have shown the bottom surface or a cut surface to be less susceptible to degradation owing to differences in properties and microstructure of the top surface compared to the bottom surface [58–60]. Fig. 10 shows the interplay between salt scaling mass loss of the top surface and segregation for air entrained and non-air entrained mixtures. When the top surface is tested, the mixtures without entrained air exceed the acceptable mass loss limit of 0.8 kg/m^2 specified by OPSS 1351 [44] well before completion of the specified 50 freeze–thaw cycles. The mass loss is reduced by almost 60% for mixtures containing entrained air. Even though SCC mixtures typically have higher cement contents and lower w/cm ratios than conventional concrete, increased air content is still essential to ensure freeze–thaw durability and salt scaling resistance. Evaluation of the top and bottom surfaces and emphasizing their differences are critical points in relation to real structures where the bottom surfaces are not typically damaged since they do not reach critical saturation. In contrast, the top surface is exposed and vulnerable to moisture and ion penetration and as a result is more vulnerable to durability related degradation.

To further examine the influence of entrained air on the scaling performance of SCC, the relationship between mortar band thickness and mass loss was examined. Fig. 11 shows the correlation between mortar band thickness and mass loss for air entrained and non-air entrained concrete. Fig. 11a shows a larger range of mortar band thicknesses and mass losses associated with the top surface compared to the bottom surface, shown in Fig. 11b. The wider range of mass loss and average mortar band thickness of the top surface is attributed to the segregation measured for the mixtures. The mixtures with entrained air exhibited better scaling resistance than the mixes without entrained air, even though the top surface had higher mortar band thicknesses. These results reveal that highly segregated mixtures as measured by column technique, VSI or V-funnel (t_5–t_0) can still exhibit good de-icer salt scaling resistance if they are adequately air entrained. In contrast, non-air entrained mixtures exhibit poor scaling resistance even though segregation measured by the column technique, VSI and V-funnel (t_5–t_0) measurements are within the acceptable limits as specified by MTO-SP-SCC [36] or EFNARC

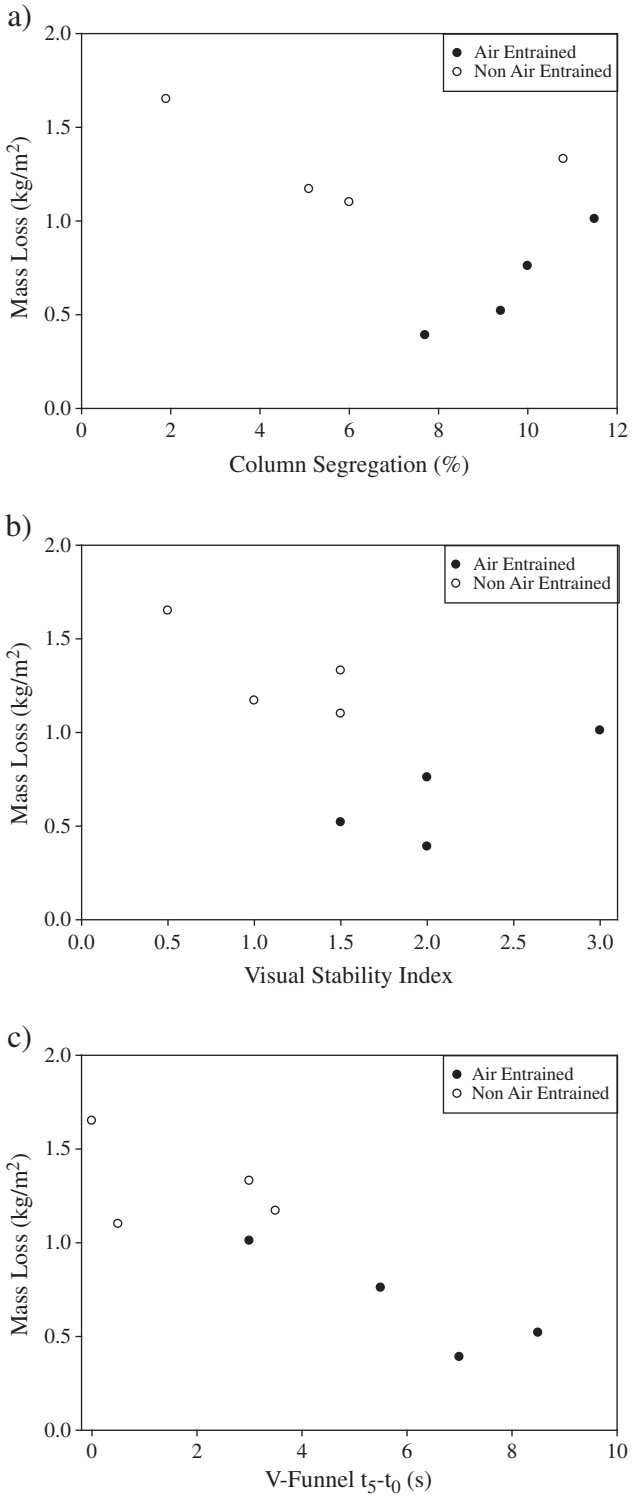

Fig. 10. The correlation between scaling mass loss and segregation measured by: a) column method, b) VSI, and c) V-funnel (t_5–t_0).

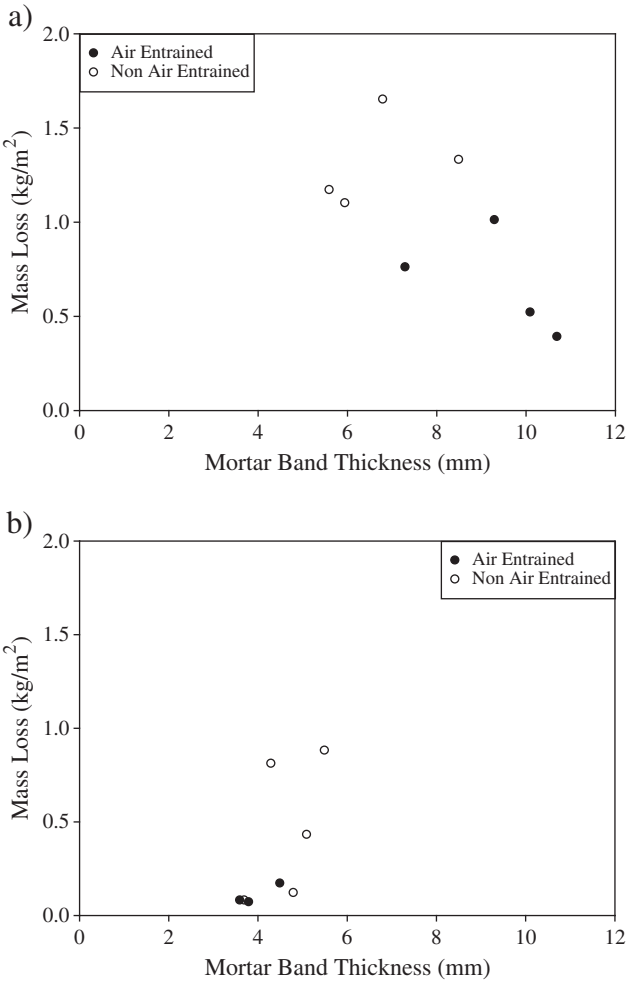

Fig. 11. Correlation between salt scaling mass loss and mortar band thickness for a) top surface and b) bottom surface.

or CSA guidelines where specified. There is, however, an increasing trend in mortar band thickness and salt scaling mass loss for non-air entrained mixtures.

5. Summary and concluding remarks

The following concluding remarks pertain to SCC that is designed with good quality materials and mix design methods but may exhibit varying degrees of segregation attributed to on-site variations in aggregate distributions, and/or chemical admixtures.

1. Relatively high segregation values did not result in reduced compressive strength or rapid chloride permeability values. For all mixes, the rapid chloride permeability was less than 1600 C, and the 7-day compressive strength for all mixes falls within the range of 44–49 MPa. The insignificant impact of poor segregation on rapid chloride permeability and compressive strength is attributed to the quality of the materials and mix proportions used in this study.
2. Air entrained mixtures exhibit greater segregation in accordance with the column technique, VSI and V-funnel (t_5–t_0) measurements but exhibit superior resistance to freeze–thaw and de-icer salt scaling damage in comparison to non-air entrained mixtures.
3. The sorptivity coefficient, de-icer salt scaling mass loss and mortar band thickness are larger for the top surface of SCC specimens in comparison to the bottom surface.
4. Determination of the mortar band thickness using digital image analysis requires strong contrast and brightness of the paste–aggregate interface. Critical sample preparation details necessary to achieve this are:
   i. Saw cut the specimen and rinse the cut face.
   ii. Pat the cut surface dry until SSD condition is achieved
   iii. Spray the freshly cut face with 1% phenolphthalein and rinse off excess solution.

iv. After at least 16 h, apply a thin coating of petroleum jelly to the surface.
v. After 5 min, wipe off the excess petroleum jelly, scan and analyze.

5. Although the hardened visual stability index (HVSI) rating reported in Fang and Labi [45] describes 'slight mortar band layer' as less than 25 mm, this study revealed that mortar bands as thin as 11 mm can exhibit relatively poor surface transport and durability properties, specifically sorptivity and de-icer salt scaling resistance, respectively.
6. The correlation between segregation and sorptivity of SCC is independent of air content. Increased segregation measured by the column method and VSI results in an increase in initial sorptivity for the top surface of a SCC specimen.
7. SCC cast with quality materials and mix proportions in accordance with current guidelines may still be vulnerable to poor segregation resistance which can result in adverse effects on surface transport properties and durability performance.

Acknowledgements

The authors would like to acknowledge the insightful discussions with Ms. H. Schell (MTO), Mr. D. Rhead (MTO), and Prof. R.D. Hooton (University of Toronto) throughout this project. Funding for this project was provided through the Ontario Ministry of Transportation's Highway Infrastructure Innovations Funding Program and the Natural Sciences and Engineering Research Council of Canada. Materials were donated by Holcim Canada and BASF Canada.

References

[1] J. Newman, B.S. Choo, Advanced Concrete Technology Processes, Elsevier Ltd, 2003.
[2] ACI 238.1R-08, Report on Measurements of Workability and Rheology of Fresh Concrete, American Concrete Institute, Farmington Hills MI, 2008.
[3] J.A. Daczko, Stability of self-consolidating concrete, Assumed or ensured? Proceedings of the First North American Conference on the Design and Use of SCC, 2002, p. 7.
[4] D. Bonen, S.P. Shah, Fresh and hardened properties of self-consolidating concrete, Prog. Struct. Eng. Mat. 7 (2005) 14–26.
[5] K.H. Khayat, A. Guizani, Use of viscosity modifying admixtures to enhance stability of fluid concrete, ACI Mat. J. 94 (1997) 332–340.
[6] H.A. Mesbah, A. Yahia, K.H. Khayat, Validation of electrical conductivity method to assess static stability of SCC, in: K. Khayat, D. Feys (Eds.), Proceedings of the SCC 2010 Volume II—Design Production and Placement of Self Consolidating Concrete, 2010, pp. 551–562.
[7] T. Krankel, D. Lowke, C. Gehlen, Direct and indirect determination of the segregation resistance of SCC, in: K. Khayat, D. Feys (Eds.), Proceedings of the SCC 2010 Volume II—Design Production and Placement of Self Consolidating Concrete, 2010, pp. 603–610.
[8] G. De Schutter, Durability of SCC—from materials to structures, in: K. Khayat, D. Feys (Eds.), Proceedings of the SCC 2010 Volume II—Design Production and Placement of Self Consolidating Concrete, 2010, pp. 47–51.
[9] V. Boel, P. Helincks, P. Desnerck, G. DeSchutter, Bond behaviour and shear capacity of self compacting concrete, in: K. Khayat, D. Feys (Eds.), Proceedings of the SCC 2010 Volume I—Design, Production and Placement of Self-Consolidating Concrete, 2010, pp. 343–353.
[10] W. Zhu, J.C. Gibbs, P.J.M. Bartos, Uniformity of in situ properties of self-compacting concrete in full scale structural elements, Cem. Conc. Comp. 23 (1) (2001) 57–64.
[11] P. Turcry, A. Loukili, K. Haidar, G. Pijaudier-Cabot, A. Belarbi, Cracking tendency of self-compacting concrete subjected to restrained shrinkage: experimental study and modeling, J. Mat. Civ Eng. 18 (1) (2006) 46–54.
[12] W. Zhu, P. Bartos, Permeation properties of self-compacting concrete, Cem. Concr. Res. 33 (2003) 921–926.
[13] H. Yazici, The effect of silica fume and high-volume Class C flyash on mechanical properties, chloride penetration and freeze–thaw resistance of self-compacting concrete, Constr. Build. Mats. 22 (2008) 356–462.
[14] V. Boel, K. Audenaert, G. DeSchutter, Gas permeability and capillary porosity of self-compacting concrete, Mat. Struct. J. 41 (2008) 1283–1290.
[15] J.M. Khatib, Performance of self-compacting concrete containing fly ash, Constr. Build. Mats. 22 (2008) 1963–1971.
[16] S.D. Hwang, K.H. Khayat, Durability characteristics of self-consolidating concrete designated for repair applications, Mat. Struct. J. 42 (2009) 1–14.
[17] K. Turk, S. Caliskan, S. Yazicioglu, Capillary water absorption of self-compacting concrete under different curing conditions, Indian J. Eng. Mat. Sci. 14 (2007) 365–372.
[18] M. Sahmaran, I.O. Yaman, M. Tokyay, Transport and mechanical properties of self consolidating concrete with high volume fly ash, Cem. Concr. Comp. 31 (2009) 99–106.
[19] A. Kanellopoulos, M.F. Petrou, I. Ioannou, Durability indicators of SCC, Proceedings of the 2nd International RILEM Workshop on Concrete Durability and Service Life Planning, 2007, pp. 286–292.
[20] EFNARC, The European Guidelines for Self-compacting Concrete Specification, Production and Use, 2005.
[21] CSA A23.1-09, Concrete Materials and Methods of Concrete Construction, Canadian Standards Association, 2009.
[22] P. Breul, J.-M. Geoffray, Y. Haddani, On-site concrete segregation estimation using image analysis, J. Adv. Concr. Tech. 6 (1) (2008) 1–10.
[23] S. Assie, G. Escadeillas, V. Waller, Estimates of self compacting concrete potential durability, Const. Build. Mat. 21 (2007) 1909–1917.
[24] Ontario Provincial Standard Specification (OPSS) 1002, Material Specifications for Aggregates – Concrete, , 2004.
[25] American Society for Testing and Materials, ASTM C33-07, Standard Specification for Concrete Aggregates, , 2007.
[26] EFNARC, Specification and Guidelines for Self Compacting Concrete, 2002.
[27] Ontario Provincial Standard Specification (OPSS) 1350, Material Specification for Concrete – Materials and Production, , 1995.
[28] D.K. Panesar, B. Shindman, Elastic properties of self consolidating concrete, Constr. Build Mater. 25 (2011) 3334–3344.
[29] Ministry of Transportation, Ontario Laboratory Testing Manual MTO LS-436 (2007) Air Content of Freshly Mixed Self-Consolidating Concrete by the Pressure Method. Ministry of Transportation, Ontario Laboratory Testing Manual.
[30] American Society for Testing and Materials ASTM C1610-06, Standard Test Method for Static Segregation of Self-consolidating Concrete Using Column Technique, 2006.
[31] Ministry of Transportation, Ontario Laboratory Testing Manual MTO LS-442 (2007) Segregation and Settlement of Freshly Mixed Self-Consolidating Concrete by the Column Method.
[32] American Society for Testing and Materials, ASTM C1611/C1611M-09, Standard Test Method for Slump flow of Self Consolidating Concrete, , 2009.
[33] Ministry of Transportation, Ontario Laboratory Testing Manual MTO LS-438 (2007) Method for Evaluation of Freshly Mixed Self Consolidating Concrete By Slump Flow.
[34] Ministry of Transportation, Ontario Laboratory Testing Manual MTO LS-441 (2007) Evaluation of Freshly Mixed SCC with the V-funnel.
[35] J. Daczko, M. Kurtz, Development of high volume coarse aggregate self-compacting concrete, Proceedings of the 2nd International Symposium on Self-Compacting Concrete. Tokyo, Japan, 2001, pp. 403–412.
[36] Ministry of Transportation, Ontario Special Provisions—Self Consolidating Concrete MTO-SP-SCC (2009) Amendment to OPSS 1350 April 2007 Draft.
[37] American Society for Testing and Materials ASTM C39-05, Standard test for compressive strength of cylindrical concrete specimens, , 2006.
[38] Ministry of Transportation, Ontario Laboratory Testing Manual MTO LS-437 (2007) Method of Making and Curing Freshly Mixed Self-Consolidating Concrete Compression Test Specimens.
[39] American Society for Testing and Materials, ASTM C1202-07 (2007) Standard Test Method for Electrical Indication of Concrete's Ability to Resist Chloride Ion Penetration.
[40] American Society for Testing and Materials, ASTM C1585-04 (2004) Standard Test Method for Measurement of Rate of Absorption of Water by Hydraulic Cement Concretes.
[41] American Society for Testing and Materials, ASTM C666-03 (2004) Standard Test Method for Rapid Freeze–Thaw Resistance of Concrete.
[42] Ministry of Transportation, Ontario Laboratory Testing Manual MTO LS-412 (1997) Method of test for scaling resistance of concrete surfaces exposed to de-icing chemicals Rev. No. 17.
[43] American Society for Testing and Materials, ASTM C672M-03 (2004) Standard Test Method for Scaling Resistance of Concrete Surfaces Exposed to De-icing Chemicals.
[44] Ontario Provincial Standard Specification (OPSS) 1351 (2004) Material Specification for Precast Reinforced Concrete Components for Maintenance Holes, Catch Basins, Ditch Inlets, and Valve Chambers.
[45] C. Fang, S. Labi, Image-processing technology to evaluate static segregation resistance of hardened self-consolidating concrete, Transp. Res. Rec.: J. Transp. Res. Board 2020 (2007) 1–9.
[46] B. Shindman, A comparative evaluation of plastic property test methods for self-consolidating concrete and their relationships with hardened properties. M. A. Sc. Thesis, Department of Civil Engineering, The University of Toronto, Toronto, Ont. (2011)
[47] B. Shindman, D.K. Panesar, A comparison of segregation test methods: visual stability index and column method, in: K. Khayat, D. Feys (Eds.), Proceedings Vol. II Self-Consolidating Concrete (SCC) 2010- Design Production, and Placement of SCC 6th International RILEM Symposium on SCC , Montreal, Quebec, Canada, 2010, pp. 563–571.
[48] A. Rosli, A.B. Harnick, Improving the durability of concrete to freezing and de-icing salts, in: P.J. Sereda, G.G. Litvan (Eds.), Proceedings of Durability of Building Materials and Components, ASTM STP 691, American Society for Testing and Materials, 1980, pp. 464–473.
[49] P.C. Kreijger, The skin of concrete: composition and properties, Mat. Struct. 17 (100) (1984) 274–283.
[50] M. Pigeon, R. Pleau, Durability of concrete in cold climates. Modern Concrete Technology 4, E&FN Spon 1995.

[51] V. Patel, A. Boyd, Sorptivity testing to assess the durability of SCC during freeze–thaw cycling, in: K. Khayat, D. Feys (Eds.), Proceedings of the SCC 2010 Volume II—Design Production and Placement of Self Consolidating Concrete, 2010, pp. 1027–1037.
[52] K.H. Khayat, B. Persson, Frost durability and salt scaling of SCC, in: G. De Schutter, K. Audenaert (Eds.), Durability of Self-compacting Concrete State-of-the-Art Report of RILEM Technical Committee 205-DSC, RILEM Publications S.A.R.L, 2007, pp. 119–136.
[53] B. Persson, Internal frost resistance and salt scaling of self-compacting concrete, Cem. Concr. Res. 33 (2003) 373–379.
[54] E.P. Koehler, D.W. Fowler, Static and dynamic yield stress measurements of SCC, SCC2008 Conference Proceedings, Chicago, Illinois, 10–12 November 10–12, 2008, pp. 1–6.
[55] E.P. Koehler, Use of rheology to specify, design, and manage self consolidating concrete, Supplementary Proceedings of the Tenth ACI International Symposium on Recent Advances in Concrete Technology and Sustainability Issues. Sevilla, Spain, 2009, pp. 1–15.
[56] R. Zerbino, B. Barragán, T. Garcia, L. Agulló, R. Gettu, Workability tests and rheological parameters in self-compacting concrete, Mat. Struct. J. 42 (2009) 947–960.
[57] J. Carlswärd, M. Emborg, S. Utsi, P. Öberg, Effect of constituents on the workability and rheology of self-compacting concrete, in: O. Wallevik, I. Nielsson (Eds.), Proceedings of the 3rd International RILEM Symposium on Self-Compacting Concrete, Reykjavik, Iceland, 17–20 August 2003, RILEM Publications S.A.R.L, 2003, pp. 143–153.
[58] K. Sakai, M. Kumagai, K. Abe, H. Endoh, Effect of pore structure on scaling deterioration of concrete, in: N. Banthia, K. Sakai, O. Ojorv (Eds.), Proceedings 3rd International Conference on Concrete Under Severe Conditions, 2001, pp. 396–403.
[59] R. Bleszynski, R.D. Hooton, M. Thomas, C.A. Rogers, Durability of ternary blend concrete with silica fume and blast-furnace slag: laboratory and outdoor exposure site studies, ACI Mat. J. 99 (5) (2002) 499–508.
[60] M. Pigeon, C. Talbot, J. Marchand, H. Hornain, Surface microstructure and scaling resistance of concrete, Cem. Concr. Res. 26 (10) (1996) 1555–1566.